To What Extent Implanting Single vs Pairs of Magnets Per Muscle Affect the Localization Accuracy of the Myokinetic Control Interface? Evidence From a Simulated Environment

Flavia Paggetti, Marta Gherardini, Alessandro Lucantonio, and Christian Cipriani

***Abstract*—*Objective:* We recently proposed a new concept of human-machine interface to control hand prostheses which we dubbed the *myokinetic control interface*. Such interface detects muscle displacement during contraction by localizing permanent magnets implanted in the residual muscles. So far, we evaluated the feasibility of implanting one magnet per muscle and monitoring its displacement relative to its initial position. However, multiple magnets could actually be implanted in each muscle, as using their relative distance as a measure of muscle contraction could improve the system robustness against environmental disturbances. *Methods:* Here, we simulated the implant of pairs of magnets in each muscle and we compared the localization accuracy of such system with the one magnet per muscle approach, considering first a planar and then an anatomically appropriate configuration. Such comparison was also performed when simulating different grades of mechanical disturbances applied to the system (i.e., shift of the sensor grid). *Results:* We found that implanting one magnet per muscle always led to lower localization errors under ideal conditions (i.e., no external disturbances). Differently, when mechanical disturbances were applied, magnet pairs outperformed the single magnet approach, confirming that differential measurements are able to reject common mode disturbances. *Conclusion:* We identified important factors affecting the choice of the number of magnets to implant in a muscle. *Significance:* Our results provide important guidelines for the design of disturbance rejection strategies and for the development of the myokinetic control interface, as well as for a whole range of biomedical applications involving magnetic tracking.**

***Index Terms*—Human-machine interface, magnetic tracking, myokinetic interface, prosthetics.**

Manuscript received 18 November 2022; revised 5 April 2023; accepted 25 April 2023. Date of publication 4 May 2023; date of current version 28 September 2023. This work was supported in part by the European Research Council through MYKI Project under Grants ERC-2015-StG and 679820, and in part by the Centro Protesi - Istituto Nazionale per L'Assicurazione Contro Gli Infortuni Sul Lavoro through MIO-PRO Project under Grant PR19-CR-P1. *(Corresponding author: Christian Cipriani.)*

Flavia Paggetti, Marta Gherardini, and Alessandro Lucantonio are with the BioRobotics Institute, Scuola Superiore Sant'Anna, Italy and also with the Department of Excellence in Robotics and AI, Scuola Superiore Sant'Anna, Italy.

Christian Cipriani is with the BioRobotics Institute, Scuola Superiore Sant'Anna, 56127 Pisa, Italy and also with the Department of Excellence in Robotics and AI, Scuola Superiore Sant'Anna, 56127 Pisa, Italy.

Digital Object Identifier 10.1109/TBME.2023.3272977

Acronyms

EDM	– extensor digiti minimi.
ED	– extensor digitorum.
FDP	– flexor digitorum profundus.
FDS	– flexor digitorum superficialis.
EI	– extensor indicis.
EPL	– extensor pollicis longus.
FPL	– flexor pollicis longus.
ECRB	– extensor carpi radialis brevis.
ECRL	– extensor carpi radialis longus.
ECU	– extensor carpi ulnaris.
FCU	– flexor carpi ulnaris.
FCR	– flexor carpi radialis.

I. Introduction

In 2017, more than 57 million people worldwide were living with limb loss, with an estimated 38% regarding uni- or bi-lateral upper limb amputations [1]. Myoelectric upper limb prostheses, which make use of surface electromyography (EMG) to decipher motor intentions, represent today one of the most widespread solutions in Western Countries. However, the reliability of this approach is challenged by many factors, among which electrode repositioning/shift, muscle fatigue and the complexity of disentangling the compound information recorded at the skin level, actually generated by multiple and largely independent control sources [2]. To mitigate these issues, several techniques have been proposed, aiming at recording the control signals closer to their sources [3], [4], as well as at increasing the number of independent signals available for control [5], [6]. Regarding the former, proposed solutions include implantable myoelectric sensors (IMES) [3], and epimysial electrodes wired through osseointegrated implants [4]. Regarding the latter, novel surgical techniques allowed to amplify the number of control sites by redirecting the nerves of the stump towards surrogate muscles (i.e., targeted muscle reinnervation (TMR) [5]), or by placing muscle grafts over severed nerve terminations to induce nerve regeneration inside them (i.e., regenerative peripheral nerve interfaces [6]). Nonetheless, in spite of such important advances, a human-machine interface that enables physiological control over a large number of Degrees of Freedom (DoFs) simultaneously remains an open challenge for biomedical engineers.

Our group proposed in 2015 a new concept of human-machine interface, named the myokinetic control interface, which is

based on the transduction of residual muscle (physical) movements into control signals for a prosthesis [7]. Specifically, this approach concerns the implant of multiple permanent magnets into the residual muscles. As the magnets would displace with the corresponding muscles following contraction, their poses (i.e., their position and orientation), localized using magnetic field sensors placed in the prosthetic socket, could be used to control the external assistive devices, e.g., an upper limb prosthesis. Such interface could potentially restore a physiological control over multiple and independent DoFs. Generally speaking, muscle contraction could be monitored by implanting and localizing one or more magnets per muscle. So far, we proofed this concept by investigating the case of a single magnet per muscle for several conditions, in both ideal and anatomical workspaces, in simulated and experimental scenarios [7], [8], [9], [10], [11]. For example, we investigated the effects of geometrical configuration, localization rate and sensor resolution on the tracking accuracy [11], [9] and defined a strategy for optimizing the spatial sensor design [8]. Moreover, we simulated the implant of multiple magnets in a workspace resembling the human forearm and assessed the localization accuracy and the maximum number of implantable magnets in three transradial amputation levels [10].

This emerging idea has started producing some impact in the community, as demonstrated by the rise of scientific papers and projects embracing the approach. The most striking one is certainly that of Moradi and colleagues, which reported in 2022 about the first human implementation of a myokinetic control interface. They implanted single magnets in three flexor muscles (FDP, FCR, FDS, acronyms in appendix) of a transradial amputee, demonstrating the clinical viability of the approach [12]. Taylor et al. [13], [14] contributed to the idea and proposed the use of pairs of magnets per muscle, to measure in-vivo tissue length. They proved real-time muscle length tracking of a turkey's gastrocnemius muscle, by monitoring the relative distance between the implanted magnets.

It is known that differential measurements are immune from common mode disturbances, hence one could argue that implanting two (or even multiple) magnets within each muscle could reduce the localization errors (or artifacts) associated to mechanical disturbances due to the compliance of body tissues. In fact, monitoring a relative distance between paired magnets would reasonably reject accidental relative movements between the sensors (in the socket) and the magnets (in the muscles). Moreover, the implant of two magnets per muscle would allow to monitor the overall contraction of the muscle, while the displacement of a single magnet would only provide a local measure of deformation. Nonetheless, doubling the number of magnets inevitably increases the computation cost and the instability of the numerical solver [9], as well as the complexity/invasiveness of the surgical procedure [10].

To the best of our knowledge, although the theoretical pros and cons of the 1-magnet (1M) and 2-magnet (2M) approaches are known, a systematic comparison of their performance is missing. Such a comparison should first be theoretical, to disentangle the effects of multiple variables on the performance of the two approaches. In particular, it should consider the effects of the number of implanted magnets, of their hypothetical trajectories, and of the measured quantity (i.e., relative displacement between paired magnets, or between the actual and initial pose of one single magnet) on the overall system accuracy. Finally, the comparison of the two approaches should both consider ideal conditions (undisturbed environment) to derive general rules, as well as non-ideal ones, by simulating realistic mechanical disturbances due to the interactions of the prosthesis and socket with the environment (e.g., socket shift when lifting a weight).

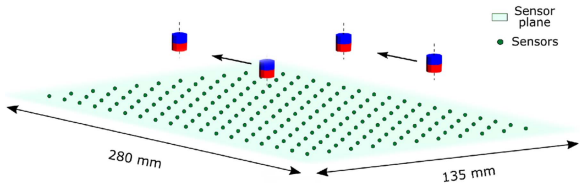

Fig. 1. Planar setup simulation: example depicting two pairs of magnets ($N = 2$), according to the 2M approach.

Under these premises, in this study we compared in simulations the localization accuracy yielded by the 1M and 2M approaches, first by considering a planar setup, to derive generic and potentially scalable results, and then an anatomical workspace resembling the human forearm. In both cases the comparison was performed under ideal/undisturbed and realistic/disturbed conditions (simulated by shifting the sensor grid). Overall, in absence of mechanical disturbances 1M always showed lower localization errors than 2M, with the anatomical case suggesting that complex magnet distributions play a key role in enhancing such differences. As expected, when the disturbances were added, the 2M significantly outperformed 1M, as the latter could not reject the disturbance. The outcomes of this work represent a necessary step to fully understand the potentialities of the system under different conditions. They provide important guidelines for the design of disturbance rejection strategies, and more in general for the development of the myokinetic control interface for prosthetic limbs or other assistive devices.

II. Materials and Methods

The magnetic field generated by cylindrical magnets (radius and height of 2 mm) was simulated through an analytical magnetic dipole model described and validated earlier [15]. The field generated by the magnets was sampled on a grid of sites, simulating sensors (inter-sensor distance 9.3 mm, as in [10]) and the samples were stored and fed to a Matlab script (MathWorks, Natick, MA), where the Levenberg-Marquardt algorithm [16] was used to estimate the magnet poses offline, akin to previous works [17], [10]. A 4 mG white gaussian noise was added to the sensor recordings, to simulate the noise associated to actual 3-axis Hall-effect sensors in a real setup, as in [17], [11], [8], [9].

A. Planar Setup: Ideal Conditions

The simulation of the planar configuration included 420 3-axis magnetic field sensors, on a rectangular grid of 135 mm $\times$ 280 mm (Fig. 1). An increasing number of magnets (or magnet pairs in 2M) N, from one to 23, was simulated on a plane parallel to the sensor grid, 20 mm above it. The value of 23 was chosen as it corresponds to the maximum number of muscles, ideally available for implantation after a distal amputation, as identified in our previous study [10]. The magnets placement fulfilled the spatial arrangement rule introduced in [11]. According to this, for each magnet accurate localizations can be achieved if the ratio between the inter-magnet distance and magnet-to-sensor distance (referred to as R) is higher or

equal than 0.6. This means that deep magnets can still be localized if sufficiently (and proportionally) distanced among each other.

For the 1M approach with N magnets, for each N one simulation was run as follows: each of the N magnets was moved, one at a time, along 11 equidistant checkpoints on the parallel plane. The total length travelled by each magnet was 10 mm, with equal steps between consecutive checkpoints. For the 2M approach, N pairs of magnets were placed on the same plane, and each pair was composed by a fixed and a moving magnet. More specifically, besides the N moving magnets of the 1M approach, N additional ones were placed 40 mm far from their respective 'partner', along the longitudinal axis of the parallel plane. The moving magnets performed the same 10 mm trajectory, one at a time, moving towards the fixed ones which were kept still during the whole simulation (Fig. 1). For both the 1M and 2M approaches, the magnetic moment vectors of all magnets always pointed towards the sensor plane. Overall, 23 different simulations were performed for both 1M and 2M, and the localization accuracies were compared pairwise. In this way the two approaches were compared, virtually fixing the number of muscles. An additional comparison fixing the number of magnets was made by matching the results from 2M with those from 1M involving even numbers of magnets, up to 30 (note, as the maximum N was set to 23, seven additional simulations were performed for this comparison).

The two comparisons (fixed muscles vs. fixed magnets) served to disentangle the error caused by the numerical solver due to the number of magnets from that purely due to the measured quantity. It is indeed known that the localization errors grow with the number of magnets [18], [17].

B. Anatomical Setup: Ideal Conditions

The 1M and 2M approaches were also compared in a simulated anatomical workspace, derived from a 3D CAD model of the human forearm, already employed in [8], [10]. To ensure realistic results from the simulations we used a 3D finite element model of muscle contraction that estimated the pose of each potential magnet site inside the muscle (described in paragraph B.2). Under these assumptions the comparison was done by fixing the number of muscles (i.e., simulating N magnets in 1M and N pairs in 2M). The comparison with fixed number of magnets was deemed unnecessary, as the general trend could be inferred already from the planar configuration. Moreover, in this case fixing N would have required the placement of single magnets in additional muscles with respect to those selected for 2M, and as such implied a comparison between different magnet trajectories and workspace geometries.

Magnets were virtually implanted along the centerlines of a certain number of the selected muscles (see below). The field generated by the magnets was sampled on a grid of 840 sensors shaped around the forearm, ideally embedded in a prosthetic socket. As in [10], a distal (T3), a central (T2) and a proximal (T1) cut were considered. All muscles used in [10] were considered eligible for the implant, with a maximum of 23 muscles in T3. For each amputation level, the number of magnets to implant was identified according to the procedure described below.

1) Muscle Selection and Magnet Placement Procedure: In the 2M approach, all eligible muscles for each amputation level initially received two magnets. The latter were respectively implanted in the points of the centerline undergoing maximum and minimum displacement according to the finite element model of muscle contraction, in order to maximize the relative displacement between paired magnets (Fig. 3(c)). Then, by exploiting such model, the trajectory covered by each magnet during maximum isometric contraction (corresponding to a fiber shortening of ∼30% [19]) was derived and divided into 11 steps. As muscle shortening does not linearly increase with the contraction degree, the displacement undergone at each step was different. The R value was computed for each magnet at each checkpoint and, in cases of magnets showing an R value below the 0.6 threshold, the one with the lowest R was removed, together with its paired magnet. Then, R was computed again for all the remaining magnets, and the same procedure was iterated until all magnets showed $R \geq 0.6$. The remaining magnet pairs were moved simulating the contraction of one muscle at a time, and the localization algorithm estimated their poses at each checkpoint. For the 1M approach, all muscles selected for the 2M approach received one magnet, namely the one virtually implanted in the point of maximum displacement, and magnets followed the same trajectories one at a time. For both the 1M and 2M approach, the magnetic moment vectors of all magnets initially pointed radially (to maximize the magnetic field measured by the sensors), whereas during muscle contraction they rotated according to the fiber rotation predicted by the muscle model.

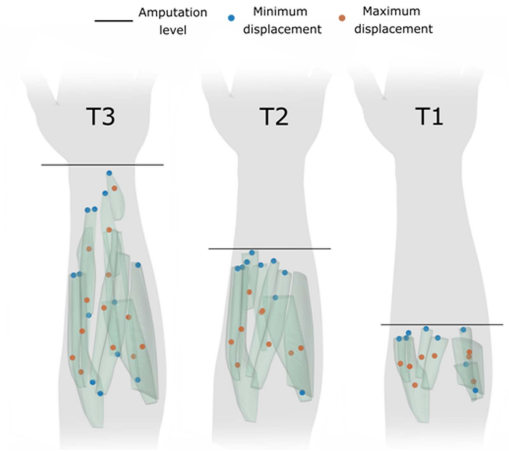

Fig. 2. Anatomical setup simulation: magnets placement in the three amputation levels. Orange dots represent sites of maximum displacement, as retrieved by the muscle model (Fig. 3): they coincide with the N magnets in the 1M approach. Blue dots represent sites of minimum displacement, or the N additional magnets included for the 2M approach.

2) Finite Element Model of Muscle Contraction: The geometry for the finite element model consisted in the muscle bellies extracted from the CAD. All tendons were removed and muscles were distally cut according to the three considered amputation levels (T1-T3). As in [10], only muscle bellies showing residual lengths of at least 20% the original ones were considered eligible for the implant; hence a different number of muscles characterized each amputation level (23 residual muscles for T3, 20 for T2, and 18 for T1) (Fig. 2). Boundary conditions were set according to common surgical anchoring techniques adopted following amputation. In particular, tendons were modeled by means of distributed springs with an elastic modulus of 800 MPa, according to the properties of healthy forearm tendons [20]. Distal tendons length depended on the amputation level. Both

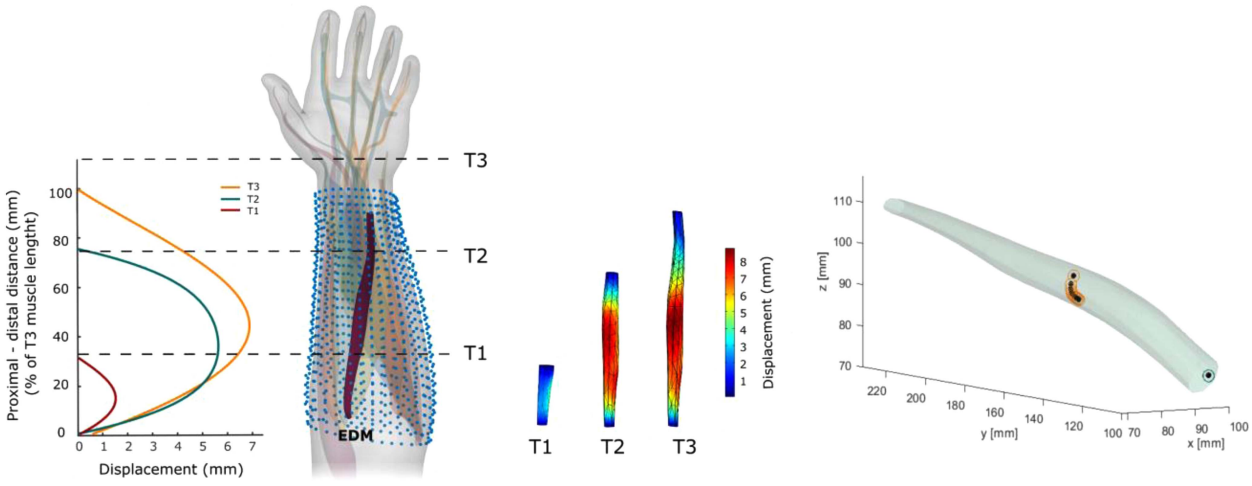

Fig. 3. Model of muscle contraction. (a) Centerline displacement of the extensor digiti minimi (EDM) for T3, T2 and T1 configurations. (b) Displacement field of EDM for T3, T2 and T1 configurations. (c) Trajectory covered by the sites of maximum (orange) and minimum displacement (blue) of the EDM during contraction, in T3.

proximally and distally (when a residual tendon was present), the spring extremity was fixed to mimic the anchoring of tendons to bones (tenodesis technique [21]). For muscles with no distal tendon left, a fixed constraint mimicking a bone anchoring was applied to their distal extremity, resembling the myodesis muscle stabilization technique [21].

A constitutive law for the muscle contraction model was implemented in a Finite Element software package (Comsol Multiphysics 5.5, COMSOL Inc., Stockholm, Sweden). Specifically, muscle bellies were modeled according to the mixture active strain approach by Riccobelli and Ambrosi [22], with parameter values according to literature (shear modulus $\mu = 30$ kPa [23], constant $I_{max} = 0.41$, fiber stiffness $\alpha = 1.5$ Mpa [24], $\beta = 1$ – related to the material stiffening behavior). The same model parameters were used for all muscles, while varying the geometries and the fiber orientation. Regarding the latter, to the best of our knowledge literature does not provide a precise orientation measure for each forearm muscle, thus it was set according to the centerline orientation of the muscle. More specifically, each centerline was defined by the interpolation of $\sim$100 points, and the vectors tangent to the centerline in those points were then interpolated (component by component) and used to define the fiber direction along the muscle. Simulations of all residual forearm muscles were performed by incrementally increasing the degree of contraction γ from 0 to 0.3 (Fig. 3(b)). The displacement of each point along the muscle centerline was derived and used to determine the magnet pose and trajectory, based on the points of maximum and minimum displacement (Figs. 2, 3(c)).

As a result of this model, the displacement of the muscle centerline was described by a bell-shaped curve as a function of the distance from the muscle origin, with the maximum approximatively located in the middle of the muscle (Fig. 3(a)). The displacement included both longitudinal and radial components, although the former was dominant. The points of maximum displacement varied across muscles and amputation levels, ranging from 1.4 mm to 11.7 mm. Generally, the points of minimum displacement coincided with the muscle extremities, which were almost fixed (0-0.3 mm range). Therefore, considering the magnet placement procedure, the distance travelled by the magnets in 1M was practically coincident with the changes in relative distance between the magnet pairs in 2M, thus making the two measures comparable also in the anatomical case.

C. Planar and Anatomical Setups: Mechanical Disturbances

The localization accuracy of the planar and of one anatomical setup was also assessed simulating the effects of external mechanical disturbances, like those potentially occurring while holding a heavy object through the end effector and prosthetic socket. In such cases the forces applied through the socket to the stump may compress its tissues, resulting into a relative movement of the sensor grid w.r.t the implanted magnets. These undesired effects were simulated by rigidly shifting the position of the sensor grid after the initial localization (calibration). More in detail, for each configuration (planar setup and T3 of the anatomical setup) three simulations, each involving a realistic shift δ of the sensor grid, from 1 to 3 mm, were performed. The sensor grid was shifted towards the magnets plane in the planar setup, and pushed against the volar side of the forearm in the anatomical setup, ideally simulating the displacement of the socket associated to the weight of a held object (Fig. 4). The magnets followed the same trajectories of the simulations under ideal conditions, and the generated magnetic field was sampled on the shifted sensor sites. Then, the Matlab script running the Levenberg-Marquardt algorithm estimated the magnet poses offline, comparing the results achieved with the disturbed and undisturbed sensor grid.

D. Performance Metrics

For the 1M approach the localization error was identified by computing the difference between the actual and estimated relative displacement of each magnet from its starting position, as in

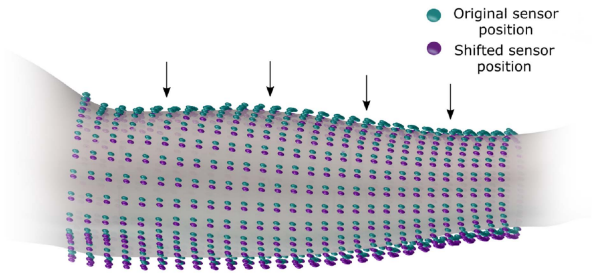

Fig. 4. Mechanical disturbances: example of sensor shift in the anatomical setup.

[7], [8], [10]. Correspondingly, the localization error was defined for the 2M approach as the difference between the actual and estimated relative distance between paired magnets at each simulation step. We also distinguished between the model error (e_m) which accounts for inaccuracies in tracking the displacement of the moving magnet, and the cross-talk error (e_{ct}) which accounts for false predictions of simultaneous displacement affecting the non-moving magnets [7]. For all configurations, localization errors from the 1M and 2M approach were statistically compared using the Wilcoxon rank sum test, as all errors proved to be not normally distributed.

III. Results

A. Ideal Conditions

1) Planar Setup: For the sake of brevity, we report the localization accuracy in retrieving the magnet positions only. The orientation errors of the 1M approach demonstrated significantly lower than those of the 2M approach ($p<0.05$), however, all proved always below 0.5° and thus unworthy to discuss.

For the 1M approach, both e_m and e_{ct} ranged between <0.01 mm and 0.15 mm, thus proving below 1.5% the trajectory covered by the magnets. For the 2M approach, all errors proved lower than ∼7% the relative displacement covered by the moving magnet, ranging between <0.01 mm and 0.70 mm (Fig. 5(a)). As a result, when comparing the two approaches considering a fixed number of muscles (thus involving N magnets in 1M and N magnet pairs in 2M), both e_m and e_{ct} of 1M proved significantly lower ($p<0.05$) for $N > 3$. Similarly, when considering the number of magnets fixed (up to 30 magnets), 1M exhibited significantly lower model errors for $N > 2$, and significantly lower cross-talk errors for $N > 4$ ($p < 0.05$) (Fig. 5(b)). However, the absolute difference between the two approaches was lower than the one found when fixing the number of muscles: for 1M all the errors demonstrated within 0.39 mm, while for 2M within 0.47 mm.

2) Anatomical Setup: Of the initial 23 (T3), 20 (T2) and 18 (T1) muscles eligible for the implant, the selection procedure identified 13, nine and eight muscles, respectively. Also in this case, we report the localization accuracy in retrieving the magnet positions only, as all orientation errors demonstrated lower than 0.5° akin to the planar simulation.

The detailed analysis of magnet displacement in the anatomical setup provides a global representation of the displacement ranges achieved by magnets/pairs and of the relationship between real and computed (localized) displacements (Fig. 6(a)). For a representative case of T3 the displacement ranged between 2.29 mm and 11.72 mm for 1M and between 2.11 mm and 10.48 mm for 2M. The pair-wise comparison highlighted that for few muscles (ECU, FCU, EDM, ECRL) the maximum Euclidean distance for 2M proved at least 25% lower than the displacement achieved for 1M (Fig. 6(a)). The relationship between real and estimated positions proved highly linear ($R^2>0.99$) for all muscles and both 1M and 2M approaches (Fig. 6(a)). The cross-talk errors demonstrated almost constant for the majority of muscles, except for the deepest muscles, i.e., ECRL and FDP-III, which proved particularly affected by the movement of other magnets, reaching errors greater than 0.5 mm in both 1M and 2M. Larger cross-talk errors in 2M were found also for ECU, FPL and FDS-II.

More in general, in T1 and T3 the average localization error for 2M was one order of magnitude larger than for 1M (average error of 0.16 mm (T1) and 0.18 mm (T3) for 2M, vs. 0.03 mm (T1) and 0.02 mm (T3) for 1M), while for T2 it increased from 0.03 mm (1M) to 0.08 mm (2M). More specifically, considering the T1 configuration (8 muscles) and the 1M approach, the 95th percentile for both e_m and e_{ct} ranged between 0.01 mm and 0.27 mm (lower than ∼5% the trajectory length covered by the magnets) (Fig. 6(b)). Differently, in the 2M approach all errors (in this section we report the error as the 95th percentile) proved lower than ∼33% the maximum variation of relative distance between paired magnets, with error values ranging between 0.02 mm and 0.56 mm, except for ECRL that reached up to 0.83 mm (Fig. 6(b)). All position errors of 1M proved statistically lower than those of 2M for all muscles ($p<0.01$).

Overall, the errors exhibited similar values and pairwise comparisons when the number of magnets hosted by the forearm increased, together with the residual limb length (T2-T3) (Fig. 6(b)). Indeed, for T2 (9 muscles) and the 1M approach errors lower than 0.32 mm (∼8% the trajectory length) were achieved, while the 2M approach showed errors up to 0.51 mm (12% the maximum change in relative distance) (Fig. 6(b)). In T3, including 13 muscles, the errors were slightly larger, albeit followed a similar trend. More specifically, while for 1M both e_m and e_{ct} demonstrated lower than 0.42 mm (∼4% the trajectory length covered by the magnets) except for the cross-talk error of FDP-III (0.51 mm, ∼22%), for 2M most of the errors exhibited greater values, i.e., up to 0.65 mm (15% the trajectory), except for FDP-III (0.78 mm, 37%) (Fig. 6(b)). Finally, the errors from the two approaches in T3 proved significantly different for all muscles ($p<0.03$), except for the cross-talk error of FCR. On the contrary, for T2 the model error relative to a subset of muscles (namely, ED-I, ECU, EDM and ECRB) were an exception to such statistical difference ($p<0.03$).

Overall, the average increase of error from 1M to 2M proved equal to 150% in the planar setup and over 400% in the anatomical one (Figs. 5-6). Moreover, comparing the performance of the planar and the anatomical setups considering the same number of magnets (8, 9 and 13 for T1, T2 and T3, respectively), the average increase of error reached 35% for 1M and over 400% for 2M.

B. Mechanical Disturbances

1) Planar Setup: Unsurprisingly, the "monopolar" localization of the 1M approach could not reject the mechanical disturbances, and the localization errors proved positively linearly correlated with the sensor grid shift δ ($r = 0.62$ for e_m) (Fig. 7). For 1M, all model errors proved below 1.07 mm for

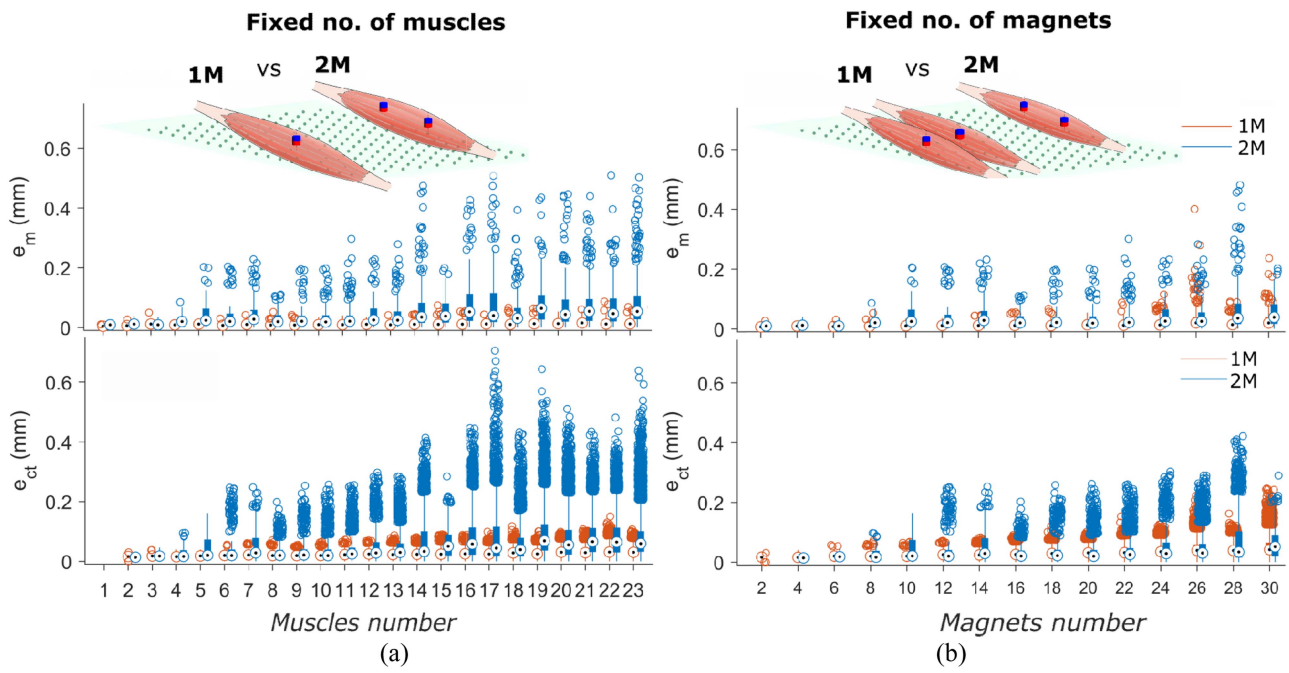

Fig. 5. Ideal planar setup results: position errors exhibited by the 1M (orange) and 2M (blue) approaches when fixing the number of muscles (a) or magnets (b). Model errors - e_m (top) and cross-talk errors - e_{ct} (bottom).

$\delta = 1$, 2.04 mm for $\delta = 2$ and 3.03 mm for $\delta = 3$. In other words, the average model error for 1M proved equal to ∼20%, 29% and 35% the disturbance intensity for δ ranging from 1 mm to 3 mm, respectively. Conversely, the differential localization used in the 2M approach rejected the adverse effects of the disturbances, as demonstrated by the lack of correlation with δ ($r<0.1$). Indeed, all error ranges proved comparable to those of the ideal scenario (Figs. 5(a), 7), proving below 0.62 mm ($\delta = 1$), 0.38 mm ($\delta = 2$) and 0.50 mm ($\delta = 3$).

2) Anatomical Setup: Again, the shift of the sensor grid yielded localization artifacts in the 1M approach, resulting in error values positively linearly correlated with the disturbance intensity ($r = 0.64$ for e_m) (Fig. 8). Indeed, for 1M the maximum e_m demonstrated 1.08 mm ($\delta = 1$), 2.17 mm ($\delta = 2$) and 3.19 mm ($\delta = 3$). It is worth noting that the model error for 1M decreased while the magnets moved along their trajectories (Fig. 8). This was caused by the way we defined the error, i.e., the difference between the actual and estimated displacements with respect to the first localization (Euclidean distances). Hence, the fixed shift of the sensor grid (δ), produced a localization error of that exact value (actual displacement = 0, estimated displacement = δ); this bias became gradually less influential as the actual displacements increased when the magnets moved along their trajectories.

The average model error of 1M proved equal to ∼61% the disturbance intensity, while the errors of 2M were not correlated to such variable ($r<0.01$) (Fig. 8, Table I). In fact, the differential measurement of the positions of magnet pairs successfully rejected the external disturbances, as all errors demonstrated below 0.8 mm. Moreover, for 2M, all errors proved similar to the results of the ideal scenario, with a comparable average and error variability (0.20±0.20 mm for $\delta = 0$, 0.17±0.17 mm for $\delta = 1$, 0.16±0.15 mm for $\delta = 2$ and 0.17±0.14 mm for $\delta = 3$) (Table I). The cross-talk error is not reported, as for 2M it demonstrated in the range of the ideal setup, while for 1M it proved simply increased by the intensity of the sensor shift δ.

TABLE I
AVERAGE E_M FOR THE 1M AND 2M APPROACHES, AS A FUNCTION OF THE SENSOR SHIFT δ

δ (mm)		0	1	2	3
1M	e_m (mm)	0.02	0.60	1.23	1.90
2M	e_m (mm)	0.20	0.17	0.16	0.17

IV. DISCUSSION

We compared the localization accuracy of the 1M and 2M approaches in a simplified planar configuration and in a relevant anatomical workspace, under ideal (undisturbed) and realistic (disturbed) conditions.

Results proved that, in the undisturbed scenario, the 2M approach led to larger localization errors compared to 1M. With respect to the position error, in the planar configuration the 1M approach provided better localization accuracies both when fixing the number of virtual muscles (N up to 23), and when fixing the number of magnets to make a matched comparison between the approaches (N up to 30) (Fig. 5). In the first case, we hypothesized that the higher error associated to the 2M approach was mainly caused by the double number of magnets involved. However, from the second analysis, it turned out that the 1M approach performed better, albeit with a smaller difference, even when an identical number of magnets. Hence, it is confirmed that the use of magnet pairs induces a propagation of the localization error. More specifically, the accuracy worsens because of a non-fixed reference for the distance computation. In fact, in the 1M approach each magnet is localized relatively to its first

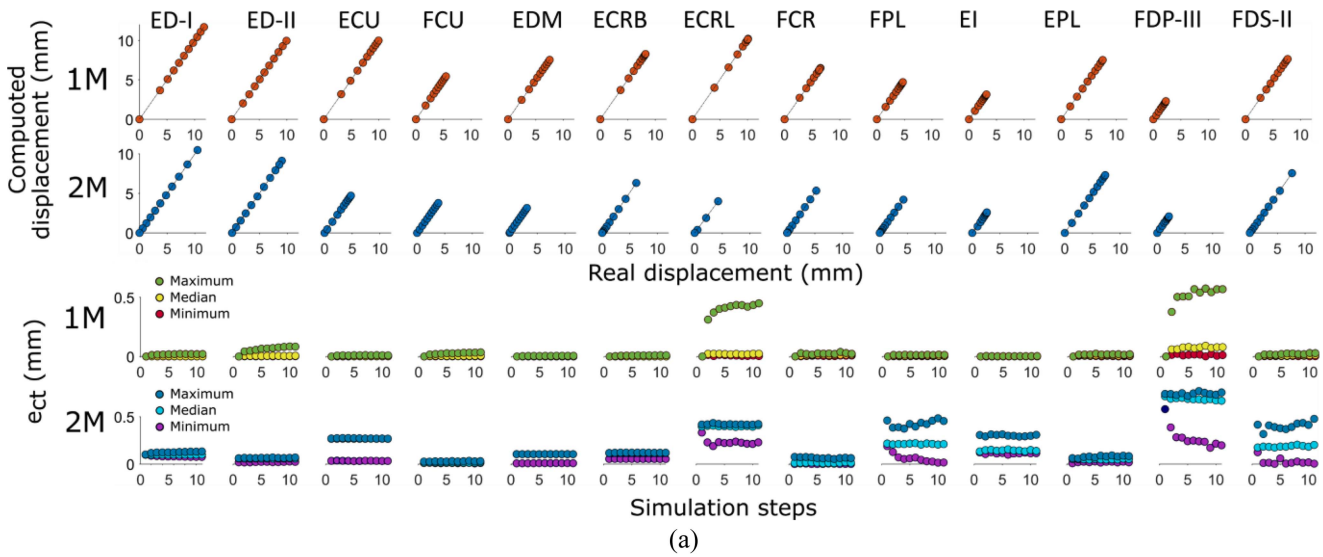

(a)

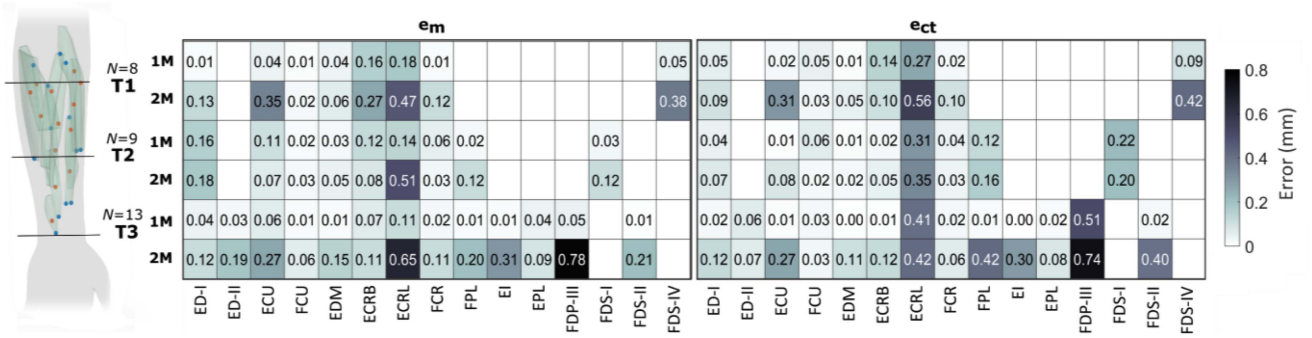

(b)

Fig. 6. Ideal anatomical setup results. (a) Representative result: real vs computed displacement for 1M and 2M in T3. (b) Comparison of the 95th percentile of position errors (e_m and e_{ct}) for the 1M and 2M approaches, in the three anatomical configurations. Acronyms in Appendix.

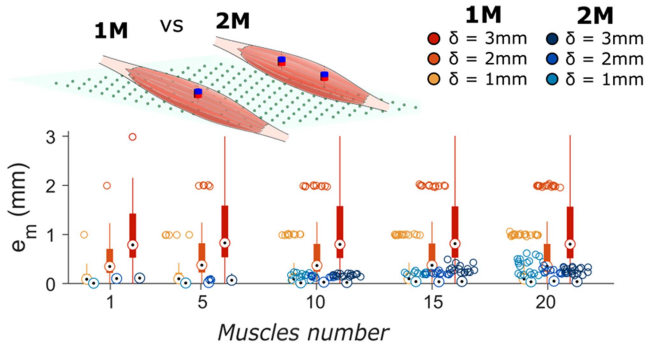

Fig. 7. Planar setup under mechanical disturbances. Model errors exhibited by representative examples from the 1M and 2M approaches (fixed number of muscles) when the sensor grid was shifted by δ.

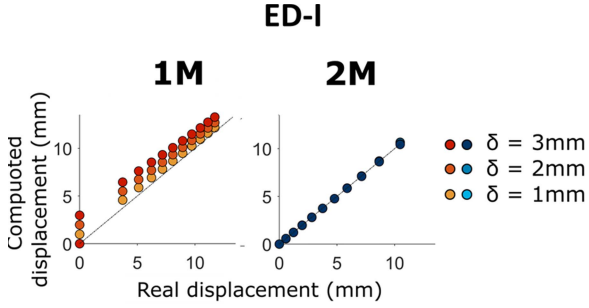

Fig. 8. Anatomical setup (T3 configuration) under mechanical disturbances. Representative results of ED-I: real vs computed displacement for 1M and 2M for the three disturbance intensities.

localization, which remains the same at each step. Instead, in the 2M approach the reference is the current localization of the second magnet of the pair, which is computed at every step and may slightly change (due to non ideal repeatability of the sensors), thus introducing an additional localization error (i.e., a measurement error). The latter sums up with the tracking error of the moving magnet, leading to a reduced localization accuracy.

The difference in localization accuracy between 1M and 2M was amplified when passing from the ideal planar to the ideal anatomical setup. We believe that was due to the more complex sensor distribution of the anatomical workspace (magnets are not always pointing towards the sensor grid) and to the geometrical placement of the magnets in space (inter-magnet and magnet-to-sensor distance).

The disturbed scenarios proved that implanting two magnets per muscle (2M) could significantly improve the localization

accuracy already when a socket shift of just 1 mm was present. Despite these findings, given the importance of the muscle geometry on the magnet placement and given the influence of the number of magnets on the computation cost of localization, the choice of implanting two magnets per muscle is still not straightforward. Indeed, also the muscle geometry and amputation level can affect the performance of the two approaches. For example, in this work the real displacement ranges were slightly different for 1M and 2M (Fig. 6(a), x axes), albeit the trajectories covered by the magnets (not considering the proximal ones in the pairs) were the same. This happens if the movement of the magnet pair is not constrained to a straight line joining the two magnets. Consequently, when a muscle shows large radial displacements, the 2M approach will inevitably lead to lower displacement ranges. This suggests that the approach to follow (1M vs 2M) should be carefully chosen also according to the main direction of deformation of the muscle. Additionally, from the finite element model we found that a decreased stump length led to progressive reductions of average and distal muscle displacements following contraction (Fig. 3(b)). We impute this to the reduced elasticity associated to shorter muscles and the stiffer distal constraints applied in proximal amputations, e.g., in T1 none of the residual muscles had a distal tendon. This suggests that, before implanting either one ore multiple magnets per muscle, the anatomy of the residual muscles, and in particular their anchoring conditions following the amputation surgery, should be attentively evaluated. Finally, this work invites further studies in which the physical interactions between magnets of different sizes and surrounding muscle tissues are modeled and comprehensively evaluated.

In the simulations we used a number of sensors larger than what could be used in an experimental validation. While one could argue that this represents a limitation w.r.t. the translation of this study towards the clinical application, it is worth noting that it might not be the case. In our previous studies we proved that the tracking accuracy when using the entire sensor grid is comparable to that obtained when using an optimal subset of the sensors [10], [11]. Eventually, as the study involves only computer simulations, an experimental validation would be beneficial. However, after having extensively experimentally validated the accuracy of our simulation models [17], [11], [9], we deemed this step unnecessary. Similarly, we did not investigate the difference in computation time for the two approaches, as the effects of the number of magnets on such variable are already known [17].

V. Conclusion

A thorough comparison of the localization accuracy of 1M and 2M suggests that: (i) implanting single magnets per muscle improves the localization accuracy in ideal scenarios, but it is not able to reject the localization artifacts induced by external disturbances on the sensor grid; (ii) the final choice of the approach (1M vs 2M) should also carefully consider the muscle mobility and anchoring conditions following the amputation, as well as the computation time requested by the application.

References

[1] C. L. McDonald et al., "Global prevalence of traumatic non-fatal limb amputation," *Prosthet Orthot Int.*, vol. 45, no. 2, pp. 105–114, 2021.

[2] A. D. Roche et al., "Prosthetic myoelectric control strategies: A clinical perspective," *Curr. Surg. Rep.*, vol. 2, 2014, Art. no. 44.

[3] R. F. Weir et al., "Implantable myoelectric sensors (IMESs) for intramuscular electromyogram recording," *IEEE Trans. Biomed. Eng.*, vol. 56, no. 1, pp. 159–171, Jan. 2009.

[4] M. Ortiz-Catalan et al., "An osseointegrated human-machine gateway for long-term sensory feedback and motor control of artificial limbs," *Sci. Transl. Med.*, vol. 6, no. 257, 2014, Art. no. 257re6.

[5] T. A. Kuiken et al., "Targeted muscle reinnervation for real-time myoelectric control of multifunction artificial arms," *J. Amer. Med. Assoc.*, vol. 301, pp. 619–628, 2009.

[6] R. C. Hooper et al., "Regenerative peripheral nerve interfaces for the management of symptomatic hand and digital neuromas," *Plast. Reconstructive Surg.*, vol. 8, no. 6, 2020, Art. no. e2792.

[7] S. Tarantino et al., "The myokinetic control interface: Tracking implanted magnets as a means for prosthetic control," *Sci. Rep.*, vol. 7, no. 1, 2017, Art. no. 17149.

[8] M. Gherardini et al., "Optimal spatial sensor design for magnetic tracking in a myokinetic control interface," *Comput. Methods Programs Biomed.*, vol. 211, 2021, Art. no. 106407.

[9] F. Masiero et al., "Effects of sensor resolution and localization rate on the performance of a myokinetic control interface," *IEEE Sensors J.*, vol. 21, no. 20, pp. 22603–22611, Oct. 2021.

[10] S. Milici et al., "The myokinetic control interface: How many magnets can be implanted in an amputated forearm? Evidence from a simulated environment," *IEEE Trans. Neural Syst. Rehabil. Eng.*, vol. 28, no. 11, pp. 2451–2458, Nov. 2020.

[11] M. Gherardini et al., "Localization accuracy of multiple magnets in a myokinetic control interface," *Sci. Rep.*, vol. 11, 2021, Art. no. 4850.

[12] A. Moradi et al., "Clinical implementation of a bionic hand controlled with kineticomyographic signals," *Sci. Rep.*, vol. 12, no. 1, Aug. 2022, Art. no. 14805.

[13] C. R. Taylor et al., "Magnetomicrometry," *Sci. Robot.*, vol. 6, 2021, Art. no. eabg0656.

[14] C. R. Taylor, H. G. Abramson, and H. M. Herr, "Low-latency tracking of multiple permanent magnets," *IEEE Sensors J.*, vol. 19, no. 23, pp. 11458–11468, Dec. 2019.

[15] N. Derby and S. Olbert, "Cylindrical magnets and ideal solenoids," *Amer. J. Phys.*, vol. 78, no. 3, pp. 229–235, 2010.

[16] J. J. Moré, *The Levenberg-Marquardt Algorithm: Implementation and Theory*. Berlin, Germany: Springer, 1978.

[17] S. Tarantino et al., "Feasibility of tracking multiple implanted magnets with a myokinetic control interface: Simulation and experimental evidence based on the point dipole model," *IEEE Trans. Biomed. Eng.*, vol. 67, no. 5, pp. 1282–1292, May 2020.

[18] L. Maréchal et al., "Design optimization of a magnetic field-based localization device for enhanced ventriculostomy," *J. Med. Devices*, vol. 10, no. 1, pp. 1–9, 2016.

[19] R. I. Griffiths, "Shortening of muscle fibers during stretch of the active cat medial gastrocnemius muscle: The role of tendon compliance," *J. Physiol.*, vol. 436, pp. 219–236, 1991.

[20] J. F. Weber et al., "Tensile mechanical properties of human forearm tendons," *J. Hand Surg.*, vol. 436, pp. 711–719, 2015.

[21] D. G. Smith et al., "General principles of amputation surgery," in *Atlas of Amputations and Limb Deficiencies: Surgical, Prosthetic, and Rehabilitation Principles*. Rosemont, IL, USA: American Academy of Orthopaedic Surgeons, 2004, pp. 21–30.

[22] D. Riccobelli and D. Ambrosi, "Activation of a muscle as a mapping of stress-strain curves," *Extreme Mechanics Lett.*, vol. 28, pp. 1–12, 2019.

[23] K. Lima et al., "Assessment of the mechanical properties of the muscle-tendon unit by supersonic shear wave imaging elastography: A review," *Ultrasonography*, vol. 37, no. 1, pp. 3–15, 2018.

[24] J. Ochala et al., "Single skeletal muscle fiber elastic and contractile characteristics in young and older men," *J. Gerontol.: Ser. A*, vol. 62, no. 4, pp. 375–381, 2007.

Open Access provided by 'Scuola Superiore "S'Anna" di Studi Universitari e di Perfezionamento' within the CRUI CARE Agreement